Structural and Optical Properties in thin-films of (GeGa2)100-x(Sb2Ga3)x (x = 15, 30, 45, 60) Alloys

Rajnish Raj
Madan Mohan Malaviya University of Technology
Pooja Lohia
Madan Mohan Malaviya University of Technology
D K Dwivedi (todkdwivedi@gmail.com)
M.M.M. University of Technology, Gorakhpur https://orcid.org/0000-0002-8334-5535

Research Article

Keywords: Non-oxide glass, Optical bandgap, FTIR, Urbach energy, Structural morphology

Posted Date: February 24th, 2021

DOI: https://doi.org/10.21203/rs.3.rs-226001/v1

Structural and optical properties in thin-films of $(GeGa_2)_{100-x}(Sb_2Ga_3)_x$ (x = 15, 30, 45, 60) alloys

Rajnish Raj[a], Pooja Lohia[a], D. K. Dwivedi[b]
[a]Department of Electronics and Communication Engineering
M. M. M. University of Technology, Gorakhpur 273010, (India)
[b]Amorphous Semiconductor Research Lab
Department of Physics and Material Science
M. M. M. University of Technology, Gorakhpur 273010, (India)

Abstract

Investigation of structural morphology and optical parameters of non-oxide $(GeGa_2)_{100-x}$ $(Sb_2Ga_3)_x$ (x = 15, 30, 45, 60) glass alloys have been studied in the present paper. Thin films of prepared bulk samples by melt quenching technique were obtained using thermal evaporation method. XRD, DSC and SEM were used to investigate the structural morphology and thermal properties of materials. The linear and non-linear optical properties of prepared samples have been studied for optoelectronic applications. FTIR transmittance spectra defines the impurities present in the prepared glassy alloys. It was observed that energy bandgap (E_g) obtain by Tauc's plot varies from 2.9 eV to 1.25 eV. The calculated value of k, E_g decreases whereas the α and Urbach energy increases with increasing doping Sb concentration. The decrease in energy bandgap is discussed on the basis of Mott and Davis model.

Keywords: Non-oxide glass, Optical bandgap, FTIR, Urbach energy, Structural morphology.

1. Introduction

The non-oxide glasses are appealing materials for various applications like distribution of thermal images,infrared power, all such optical Raman amplification, optical switching limiting, etc [1]. All these glasses are extremely photosensitive and mechanisms of photosensitivity is due to changes impacting local materials and these materials are complex to transforming its thermal, photochemical and photo-structural, electrical, electro-optic phenomena. The function of

eachkind of mechanism depends on various functions such as the sample preparation process, excitation wavelengths and so on. The most important photoinduced alterations of glasses are shown in physical thickness by chalcogenide (volume modifications such as photo-expansion or photo-contraction), photo-darkening, (PD) (red shift in the gap in the band) and changes in photoinduced the band state of phase [2]. Such effects are preferred in glasses of chalcogenide due to structural flexibility with elevated lone-pair (p states) in the valence band [3]. In amorphous glasses, the photoinduced effects of glasses are becoming an important issue for investigation because of itspotential use for optoelectronics of such effects (photoresists, memory optics, optoelectronic circuits, etc.) [4-6].

Stated by A.S Tverjanovicha et al in Ga-Ge-S, energy exposure is greater than that of band gap resulting in the substitution of S by Se leads to photoinduced bleaching and concerning photo-induced darkening. Exposure to energy, $Ge_{20}Se_{72.5}Bi_{7.5}$ films contributes to a decrease in the optical values of the bandgap [7]. The $Ga_5Sb_{10}Ge_{25}Se_{60}$ glass is very stable for crystallization and has a high temperature transition glass, making it a suitable candidate for the development and manufacturing of IR optical devices [8]. The transformation phase of the Ge-Sb-S non-oxide glasses has recently been reported [9]. Ge-Sb-S glassy films are thereforeof particular interest because those who have received a remarkable application also as antioxidants over cladding layers of micro-resonator-based sensing [10-11].

Several other glasses compositions such as $Ge_{11.5}As_{24}Se_{64.5}$, $Ge_{10}As_{35}Se_{55}$ and Ge-As-Se have also been shown to significantly boost properties such as high nonlinearity and photo stability [4]. However, Arsenic is toxic and environmentally un-recognized when As-based devices are disregarded, Antimony is an acceptable element. It has been found that the Sb transmission line can strengthen the optical nonlinearity of the glasses due to the more ionic

existence of Sb [12]. In this work, we focused on Ga and Sb-doped $(GeGa_2)_{100-x}(Sb_2Ga_3)_x$ (x = 15, 30, 45, 60) glass alloys system designed to discover for glass both with lower T_g and higher T_c, which is important for both the active and passive optical fibre drawing. The compositional dependence of parameters such as T_g, T_c, and the optical band gap was investigated. The thermal and optical effects of the addition of Sb to the $(GeGa_2)_{100-x}(Sb_2Ga_3)_x$ (x = 15, 30, 45, 60) have been comprehensively analyzed by means of DSC, UV-VIS and optical spectra of FTIR.

2. Experimental

These glasses were processed through the melting of compounds of strong purity (5 N) elements of Ge, Ga, and Sb in the evacuated elements ($<10^5$ mbar) and silica tubes flame-sealed in a rocking furnace. The mixture was molted in a muffle furnace for 12 h at 850 °C. The tubes were retained for a further 1h at this temperature. After that, the molten tubes were quenched in ice-cooled water after freezing and formed homogenization. To achieve strong homogenization of the glasses were the oven was rocked slowly during the time the ampoule was at high temperatures, producing glass with uniform compositions [13].

Study on photo-induced development in optical properties was carried out on thermal evaporated techniquewhich produces thin films have vacuum at pressure of 10^6mbar. All the thin films have thickness 500 nm and were deposited at the rate of deposition controlled at 5MHz using a quartz crystal monitor deposited on glass substrate.

First X-ray diffractometer measurements were analyzed for all the bulk samples. X'Pert Pro of Cu-ka (1.54056 Å) emits light radiation with such a 0.2 ° step in the scanning range of 10° to 80° here. Using the technique of differential scanning calorimetry, DSC thermograms were collected (SHIMADZU DSC-60 Plus) of the as prepared samples. All observations were measured at room temperature. Using the ultraviolet-visible-near-infrared (UV-VIS)

spectrophotometer (SHIMADZU UV-2600) in the 400-1000nm range, the absorbance and transmittance spectra of the samples were reported. In the range (400-5500 cm^{-1}) of samples, the IR transmission spectrum was obtained.

3. Results and discussion

3.1. Structural properties

The measurement of the X-Ray diffraction as prepared $(GeGa_2)_{100-x}(Sb_2Ga_3)_x$ (x = 15, 30, 45, 60) material was recorded at an angle 2θ between 10^0 and 80^0 values.. From Fig1absence of any sharp peak in the pattern of XRD shows the amorphous nature of the material. SEM (Scanning Electron Microscopy) is a tool which gives the data of surface morphology of the prepared alloys. It is clear from Fig 2 that the uneven edges of the specimens correspond to the amorphous existence of the particles.

3.2. Thermal property

A Differential Scanning Calorimetry is a strong method for estimating the sample's heat flow tochange thetemperature. The DSC method also could be expanded to provide an understanding of various thermo-dynamic transitions that allows us to determine the T_g (Glass Transition Temperature), T_c (Crystalline Temperature) and T_m (Melting point Temperature) of the $(GeGa_2)_{100-x}(Sb_2Ga_3)_x$ (x = 15, 30, 45, 60) sample under study. A DSC (Differential Scanning Calorimetry) thermogram of all the selected samples is shown in Fig 3(a-d). From Fig 3(a-d) it was noticeable that there are two distinct characteristic points of the DSC thermogram, namely T_g and T_c.

All values of T_g and T_c compute from the DSC thermograms are shown in the table1 at a heating rate of 20 K/ min for the studied sample. Table 1 shows that the glass alloys $(GeGa_2)_{100-x}(Sb_2S_3)_x$, the glass transition temperature has a calculated maximum value for x= 60. T_g is

observed to increases as the concentration of doping of x increases (for x = 15 to x = 60). It can therefore be observed that in the prepared sample, Sb performs a dual behaviour. The variability in temperature of the glass transition temperature could be attributed to the bond energy difference shown in Table 2.An significant parameter for analyzing glasses is thermal stability. To evaluate the thermal stability of these glasses, multiple parameters are used. The two most popular parameters differences between the value T_g and T_c and the second criterion are the Hruby parameter, which gives the ability to forming glass [13]. The greater difference between the computed value of T_c and T_g suggests that the crystallization kinetic resistance is higher or vice versa.These glasses exhibit the crystallization peak near the temperature of the glass transition, they are considered unstable glasses, whereas glasses with a peak near the temperature of melting are considered stable glasses.Since the greater difference between T_c and T_g is x = 60, suggesting the limit of the K parameter. Therefore, $(GeGa_2)_{40}(Sb_2S_3)_{60}$ has optimum thermal stability and, therefore, the ability to form large glass.

3.3. Optical properties

3.3.1. Absorption coefficient and optical band gap analysis

Theabsorption coefficient (α) and transmission (%T) which are recorded from UV-Vis spectrophotometer for all thin film samples $(GeGa_2)_{100-x}(Sb_2Ga_3)_x$ (x = 15, 30, 45, 60). The recorded transmittance% spectra of the as prepared thin film of $(GeGa_2)_{100-x}(Sb_2Ga_3)_x$ (x = 15, 30, 45, 60) is shown in Fig 4. Due to the doping of Sb constituent the transmission % of thin film is reduced. It is also possible to investigate the electronic characteristics of the material by optimizingessential parameters for electronic transitions, widely used optical absorption measurement procedure. In order to obtain the absorption coefficient (α), UV-Vis spectrum of

absorption of the thin films as prepared has been recorded, recognizing that the band gap couldbe calculated by well-known Tauc plot model [14]

The coefficient of absorption (α) is followed by [15-17]

$$\text{Absorption coefficient } (\alpha) = 2.303 \times \frac{\text{Absorbance}}{\text{Thickness of the film}} \quad (1)$$

where,

$$\text{Absorbance} = 2 - \log (\%\text{Transmittance}) \quad (2)$$

All thin film samples are monitored for thickness by means of quartz crystal thickness monitor which was attached in setup of vacuum coating unit. Photon energy variance alpha for $(GeGa_2)_{100-x}(Sb_2Ga_3)_x$ (x = 15, 30, 45, 60) thin film was shown in Fig 5. This was noticeable that photon energy (hν) along with alpha (α) increases exponentially. Fig 5 shows evident that α increases exponentially.

The significance of E_g was calculated using Tauc plot [14] for the content under observation until alpha is known. $(\alpha h\nu)^{1/n}$ and hν plot is shown in Fig 6. Tauc's relation can be expressed as

$$(\alpha h\nu)^{1/n} = A(h\nu - E_g) \quad (3)$$

where, E_g is the distance of the optical band gap, ν defines the frequency of emitted photon, h is the constant of Plank, and A is a constant normally associated with the parameter of edge width reflecting thin film quality. The transition from n with a value of 1/2, 2, 3 and 3/2 defines the direct allowed transition, the indirect allowed transition, indirect forbidden transition and the direct forbidden transition respectively. In the current case the best match for n= 1/2 is at λ = 500 nm. So, there is a clear direct allowed transition in the studied sample.

In order to find out the value for E_g along with the Tauc map, the linear region of such curves is interpreted as the photon energy axis (hν), where it cuts the axis of energy which

provides optical band gap for the materials. The band gap for $(G_eG_{a2})_{100-x}(Sb_2Ga_3)_x$ (x=15, 30, 45, 60) is given in Table 3. It's clearly visible where the optical band gap decreases as Sb concentration increases. A well-known Mott and Davis [18] method where the density of defect states could determine the significant decrease of the band gap with increased the concentration of Sb. Such deficiencies are responsible for the localized states in the bandgap of the amorphous semiconductors. As concentration of Sb is increased, there are a more number of defect states that cause the material band gap to decrease. The present finding is in good accordance with the findings previously stated by other researchers [19-22, 23–27].

There are three distinct regions of amorphous materials for optical spectra of absorption.

I. $\alpha \leq 10^2$ cm^{-1}, haveregion of low energy of absorption.

II. Defects and impurities are present in this area. There is low energy of absorption is not determinedin this research work.

III. $\alpha \geq 10^4$ cm^{-1} is a region of higher absorption where E_g takes place in between the conduction band and the valance band.

IV. $\alpha = 10^2–10^4$ cm^{-1}, describing the Urbach exponential tail. According to the expression area of absorption depends exponentially on photon energy.

$$\alpha \sim \exp[A(h\nu - h\nu_o)]/KT \quad (4)$$

Where A = constant having the unity order, and v_o is the lowest frequency of excitonic.

The empirical correlation Urbach's, its band tail width from each localized states (E_u) close to the band edges could be determined as

$$\alpha = \alpha_0 \exp(h\nu/E_u) \quad (5)$$

where, α_0 is a constant while E_u stand for energy of Urbach. Fig.7. shows the synthesized thin film which describes the variation between ln(α) and photon energy (hν).

The reciprocal of the slopes of linear region of the graph ln (α) versus the photon-energy (hv) graph was evaluated as Urbach energy (E_u). Urbach energy (E_u) represents the enhancement of the absorption edge.

The optical band gap (E_g) is accepted to decrease when the energy of Urbach (E_u) increases significantly with the high doping concentration of Sb which is shown by Fig 8. The decrease in band gap with the higher doping concentration of Sb may be due to an increase in grain sizes and a decrease in thin film structural impairment.

3.3.2. Extinction coefficient analysis

The extinction coefficient is a fundamental optical parameter. Itmeasures the behavior of decrease in the emitting light due to absorption coefficient and attenuation and can be calculated using the accompanying formula[28]

$$k = \frac{\alpha\lambda}{4\Pi} \tag{6}$$

where α states absorption coefficient of thin film and λ provides the data incident wavelength in the thin films. The incident wavelength (λ) vs extinction coefficient (k) shows in Fig 9.

3.3.3. Infrared optical transmission spectra

Fig 10 shows the able to prepare IR optical transmission spectra $(GeGa_2)_{100-x}$ $(Sb_2Ga_3)_x$ (x = 15, 30, 45, 60) glass alloys. In the present work, the addition of Sb, it is mentioned that the transmission of the glass system is increasing. Depending on the IR transmission spectra, the absorptionbandof the as prepared sample are obtained due to its extrinsic impurities. It is clear that there may be no band of absorption in the spectral region from 3600–5400 cm^{-1} which could be support for IR transmitting applications [29-31]. The highest and most intensive band appears in the range from 2230–3580 cm^{-1} with a minimum peak of 3590 cm^{-1}. These absorption bands emerge due to external impurities that are referred to variations in the Ge-O, Ga-O bonds. A

further low absorption band found with absorbed molecular H_2O occurred approximately 3580 cm^{-1}.

4. Conclusion

High purity $(G_eG_{a2})_{100-x}$ $(Sb_2Ga_3)_x$ (x = 15, 30, 45, 60) 5N (99.999 %) alloy were synthesized using the conventional melt quenching technique. Amorphous bulk glasses $(G_eG_{a2})_{100-x}$ $(Sb_2Ga_3)_x$ (x = 15, 30, 45, 60) were used to thermal evaporation technique for synthesis thin films. The measured value of k, E_g decreases while alpha (E_u) increases with increased concentration of doping Sb. Mott and Davis Defect Density Model were used to examine the decrease in the optical band gap with an increase in Sb concentration. The investigated materials could be a good contender for applications in infrared devices. It was noted that the maximum transition in optical constants occurs at x=15. So, $(G_eG_{a2})_{100-x}$ $(Sb_2Ga_3)_x$ is the adaptive composition of IR devices.

References

[1] Nicolas Hô, Jacques M. Laniel, RéalVallée, Alain Villeneuve, Optics Letters 28(2003) 965.

[2] F. Kyriazis, S.N. Yannopoulos, Applied Physics Letters 94 (2009) 101901.

[3] Xianghua Zhang, Hongli Ma, Jean-Luc Adam, Jacques Lucas, Guorong Chen, Donghui, Materials Research Bulletin 40 (2005) 1816.

[4] M.S. Iovu, P. Boolchand, D.G. Georgiev, Journal of Optoelectronics and Advanced Materials 7 (2005) 763.

[5] A.A. Othman, H.H. Amer, M.A. Osman, A. Dahshan, Radiation Effects & Defects in Solids 159 (2004) 659.

[6] P.K. Dwivedi, S.K. Tripathi, A. Pradhn, Kulkarni, S.C. Agarwal, Journal of Non-Crystalline Solids 266–269 (2000) 924.

[7] A.S. Tverjanovicha, Glass physics and chemistry 32 (2006) 677.

[8] R. Tintu, V.P.N. Nampoori, P. Radhakrishnan, Sheenu Thomas "Photoinduced changes in optical properties of Ga–Sb–Ge–Se glasses" Optics Communications 284 (2011) 222–225.

[9] Z.B. Li, C.G. Lin, G.S. Qu, Q.H. Nie, T.F. Xu, S.X. Dai, Phase separation in non-stoichiometry Ge- Sb- S chalcogenide glasses, J. Am. Ceram. Soc. 97 (2014) 793–797.

[10] C.G. Lin, Z.B. Li, S.X. Gu, H.Z. Tao, S.X. Dai, Q.H. Nie, Laser-induced phase transformation in chalcogenide glasses investigated by micro-Raman spectrometer, J. Wuhan Univ. Technol. 29 (2014) 9–12.

[11] N. Carlie, J.D. Musgraves, B. Zdyrko, I. Luzinov, J.J. Hu, V. Singh, A. Agarwal, L.C. Kimerling, A. Canciamilla, F. Morichetti, A. Melloni, K. Richardson, "Integrated chalcogenide waveguide resonators for mid-IR sensing: leveraging material properties to meet fabrication challenges", Opt. Express 18 (2010)26728–26743.

[12] Su, X., Wang, R., Luther-Davies, B., & Wang, L. (2013). The dependence of photosensitivityon composition for thin films of $Ge_xAs_ySe_{1-x-y}$ chalcogenide glasses. Applied PhysicsA, 113(3), 575-581.

[13] Raj R, Lohia P, Dwivedi DK. Investigation of structural and optical properties of $(GeS_2)_{100-x}$ $(Sb_2S_3)_x$ (x= 15, 30, 45, 60) chalcogenide glasses for mid infrared applications. Optik. 2020 Jun 11:165041.

[14] J. Tauc, Amorphous and Liquid Semiconductors, Plenum, New York, 1974, p. 171.

[15] R. Swanepoel, Determination of surface roughness and optical constants of inhomogeneous amorphous silicon films, J. Phys. E 17 (10) (1984) 896.

[16] Mousa M.A. Imran, Omar A. Lafi, Electrical conductivity, density of states and optical band gap in $Se_{90}Te_6Sn_4$ glassy semiconductor, Physica B Condens. Matter 410 (2013) 201–205.

[17] Pravin Kumar Singh, S.K. Tripathi, D.K. Dwivedi, Effect of thermal annealing on structural and optical properties of in doped Ge-Se-Te chalcogenide thin films, Mater. Sci. 37 (4) (2019) 554–562.

[18] N.F. Mott, E.A. Davis, Electronics Processes in Non – Crys Mat, Clarendon, Oxford, 1979, p. 428.

[19] Z.B. Li, C.G. Lin, G.S. Qu, Q.H. Nie, T.F. Xu, S.X. Dai, Phase separation in non-stoichiometry Ge- Sb- S chalcogenide glasses, J. Am. Ceram. Soc. 97 (2014) 793–797.

[20] C.G. Lin, Z.B. Li, S.X. Gu, H.Z. Tao, S.X. Dai, Q.H. Nie, Laser-induced phase transformation in chalcogenide glasses investigated by micro-Raman spectrometer, J. Wuhan Univ. Technol. 29 (2014) 9–12.

[21] N. Carlie, J.D. Musgraves, B. Zdyrko, I. Luzinov, J.J. Hu, V. Singh, A. Agarwal, L.C. Kimerling, A. Canciamilla, F. Morichetti, A. Melloni, K. Richardson, "Integrated chalcogenide waveguide resonators for mid-IR sensing: leveraging material properties to meet fabrication challenges", Opt. Express 18 (2010) 26728–26743.

[22] L. Petit, N. Carlie, F. Adamietz, M. Couzi, V. Rodriguez, K.C. Richardson, Correlation between physical, optical and structural properties of sulfide glasses in the system Ge–Sb–S, Mater. Chem. Phys. 97 (2006) 64–70.

[23] J.D. Musgraves, N. Carlie, J. Hu, L. Petit, A. Agarwal, L.C. Kimerling, K.A. Richardson, Comparison of the optical, thermal and structural properties of Ge-Sb-S thin films deposited using thermal evaporation and pulsed laser deposition techniques, Acta Mater. 59 (2011) 5032–5039.

[24] C.C. Huang, C.C. Wu, K. Knight, D.W. Hewak, Optical properties of CVD grown amorphous Ge-Sb-S thin films, J. Non-Cryst. Solids 356 (2010) 281–285.

[25] S.S. Song, N. Carlie, J. Boudies, L. Petit, K. Richardson, C.B. Arnold, Spin-coating of Ge23Sb7S70 chalcogenide glass thin films, J. Non-Cryst. Solids 355 (2009) 2272–2278.

[26] J. Novak, S. Novak, M. Dussauze, E. Fargin, F. Adamietz, J.D. Musgraves, K. Richardson, Evolution of the structure and properties of solution-based Ge23Sb7S70 thin films during heat treatment, Mater. Res. Bull. 48 (2013) 1250–1255.

[27] P. Knotek, J. Navesnik, T. Cernohorsky, M. Kincl, M. Vlcek, L. Tichy, Ablation of (GeS2)(0.3)(Sb2S3)(0.7) glass with an ultra-violet nano-second laser, Mater. Res. Bull. 64 (2015) 42–50.

[28] Ahmed Saeed Hassanien, Ishu Sharma, Optical properties of quaternary a-Ge15-xSbxSe50Te35 evaporated thin films: refractive index dispersion and single oscillator parameters, Optik-International Journal for Light and Electron Optic 200 (2020) 163415.

[29] Petr Němec, M. Olivier, Emeline Baudet, Andrea Kalendova, Petr Benda, Virginie Nazabal, Optical properties of $(GeSe_2)_{100-x}(Sb_2Se_3)_x$ glasses in near-andmiddle-infrared spectral regions, Mater. Res. Bull. 51 (2014) 176–179.

[30] E.M. Vogel, M.J. Weber, D.MonKrol, Nonlinear optical phenomena in glass, Phys. Chem. Glasses 32 (6) (1991) 231–254.

[31] Nathan Carlie, N.C. Anheier Jr., Hong Amy Qiao, B. Bernacki, Mark C. Phillips, Laticia Petit, Jonathan D. Musgraves, Kathleen Richardson, Measurement of therefractive index dispersion of As2Se3 bulk glass and thin films prior to and after laser irradiation and annealing using prism coupling in the near-and mid-infraredspectral range, Rev. Sci. Instrum 82 (5) (2011) 053103.

Figure Captions

Fig 1. X-Ray Diffractogram pattern of $(GeGa_2)_{100-x}(Sb_2Ga_3)_x$ (x = 15, 30, 45, 60) glasses.

Fig 2. SEM (Scanning Electron Microscope) of $(GeGa_2)_{100-x}(Sb_2Ga_3)_x$ (a) x=15, (b) x=30, (c) x=45, (d) x=60.

Fig 3. DSC thermo-graph of $(GeGa_2)_{100-x}(Sb_2Ga_3)_x$ at 20 k/min heating rate (a) x = 15 (b) x = 30 (c) x = 45 (d) x = 60 non-oxide alloy.

Fig 4. The spectral variation of the %Transmission for prepared thin films $(GeGa_2)_{100-x}(Sb_2Ga_3)_x$ for (x = 15, 30, 45, 60).

Fig 5. The distribution of "α" varies photon energy "hν" (eV) of $(G_eG_{a2})_{100-x}(Sb_2Ga_3)_x$ (x = 15,30, 45, 60).

Fig 6. Variation between photon energy (hν) vs $(\alpha h\nu)^{1/n}$ of $(GeGa_2)_{100-x}(Sb_2Ga_3)_x$ (x = 15, 30, 45, 60).

Fig 7. Varriation of photon energy vs ln(α) of $(G_eG_{a2})_{100-x}(Sb_2Ga_3)_x$ thin films glassy alloy.

Fig 8. Shows the variation of Sb concentration E_g and E_u for $(G_eG_{a2})_{100-x}(Sb_2Ga_3)_x$ (x = 15, 30, 45, 60) E_g and E_u.

Fig 9. Variations between coefficient of extinction "k" vs wavelength "λ" of $(G_eG_{a2})_{100-x}(Sb_2Ga_3)_x$ (x = 15, 30, 45, 60).

Fig 10. IR transmittance spectra of $(G_eG_{a2})_{100-x}(Sb_2Ga_3)_x$ (x = 15, 30, 45, 60) glassy thin films.

Figures

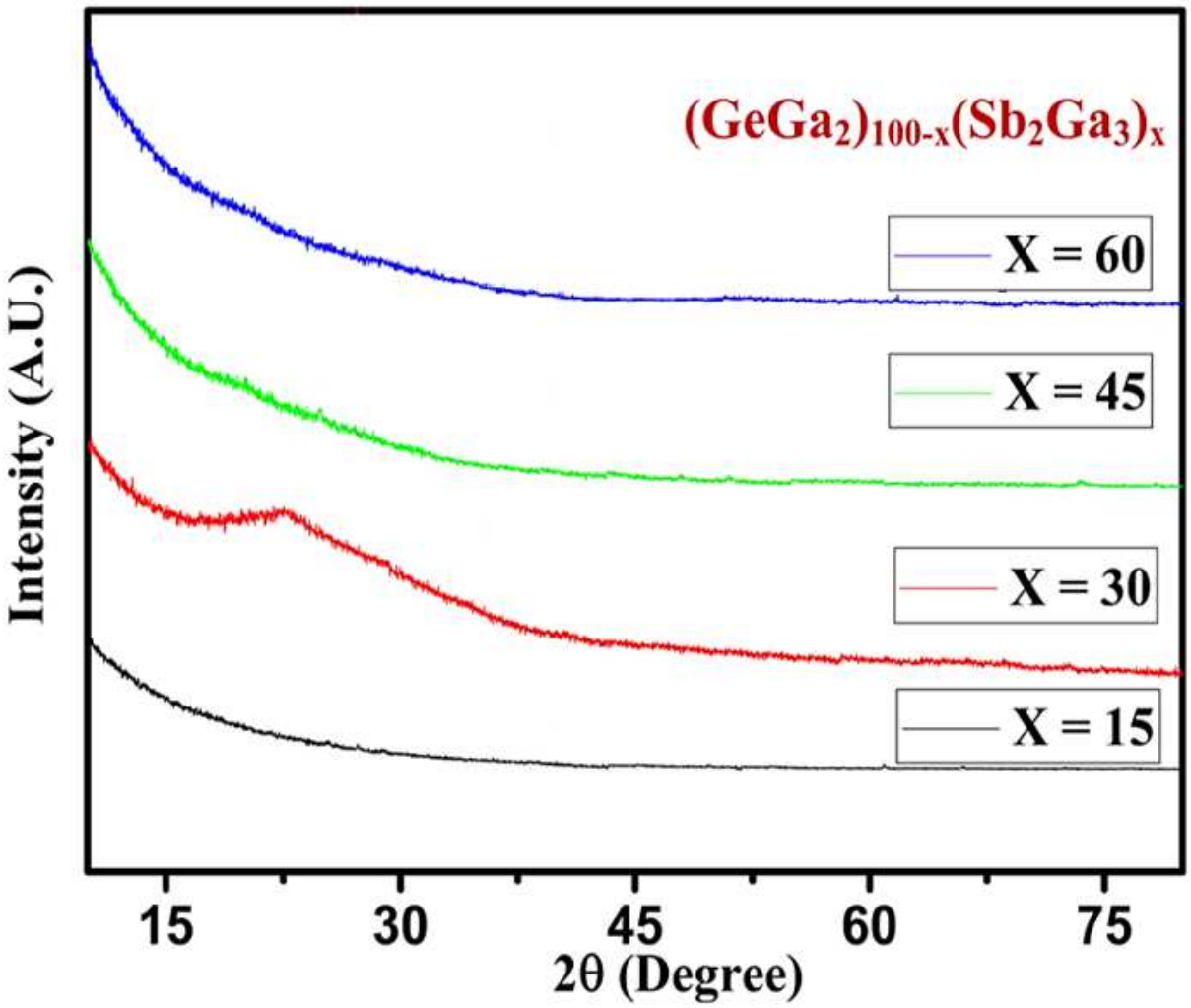

Figure 1

X-Ray Diffractogram pattern of (GeGa2)100-x(Sb2Ga3)x (x = 15, 30, 45, 60) glasses.

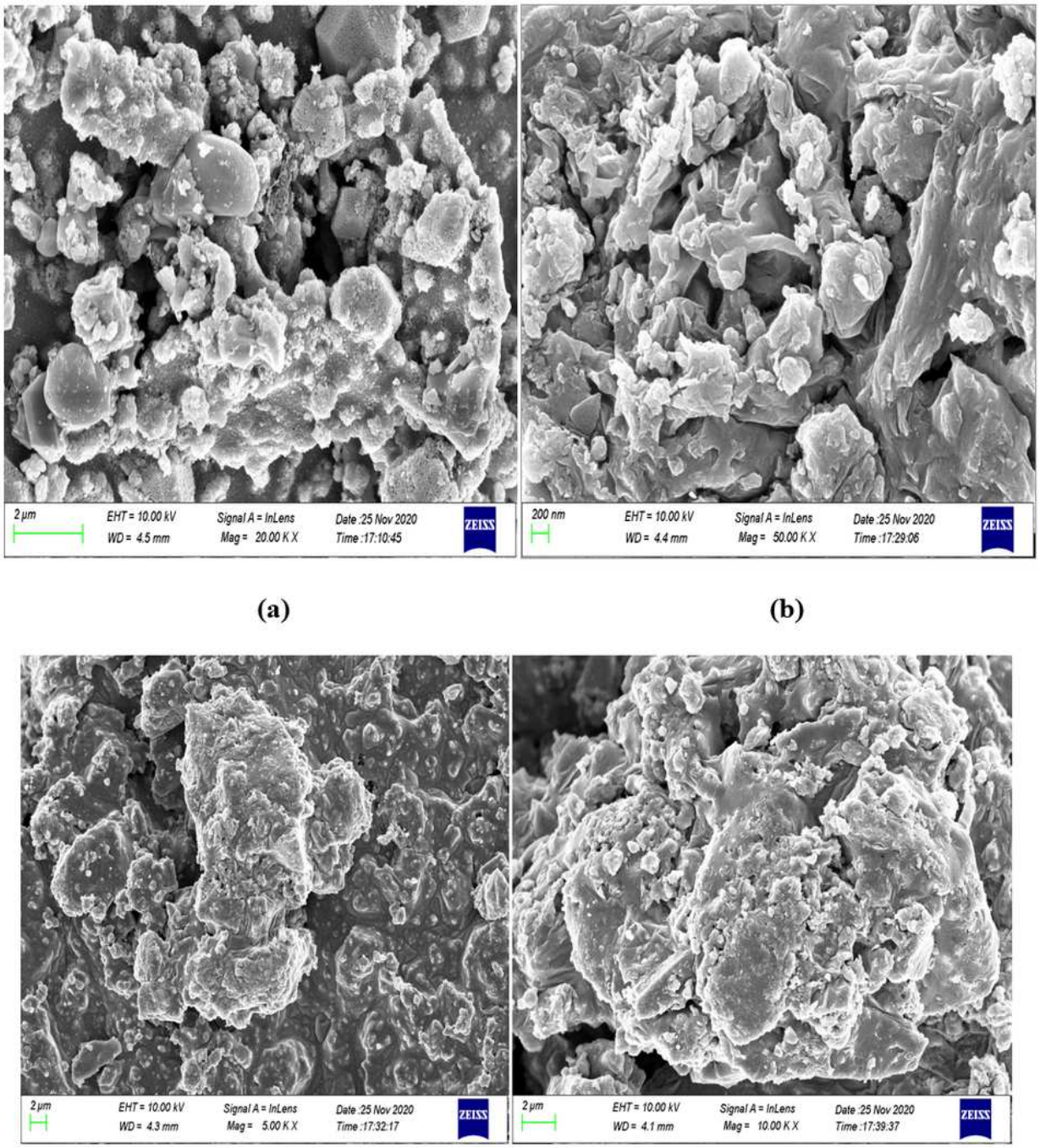

Figure 2

SEM (Scanning Electron Microscope) of (GeGa2)100-x(Sb2Ga3)x (a) x=15, (b) x=30, (c) x=45, (d) x=60.

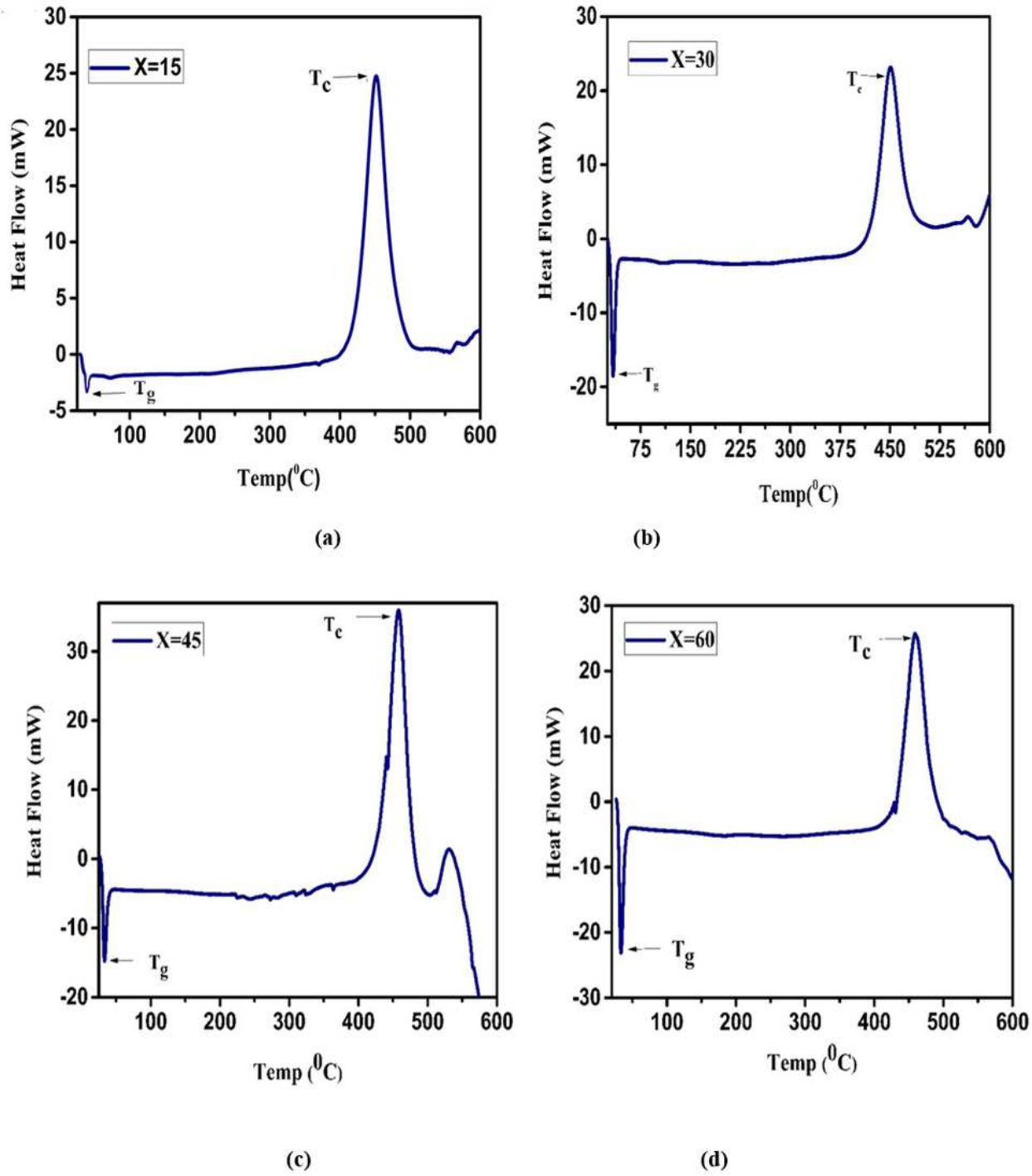

Figure 3

DSC thermo-graph of (GeGa2)100-x(Sb2Ga3)x at 20 k/min heating rate (a) x = 15 (b) x = 30 (c) x = 45 (d) x = 60 non-oxide alloy.

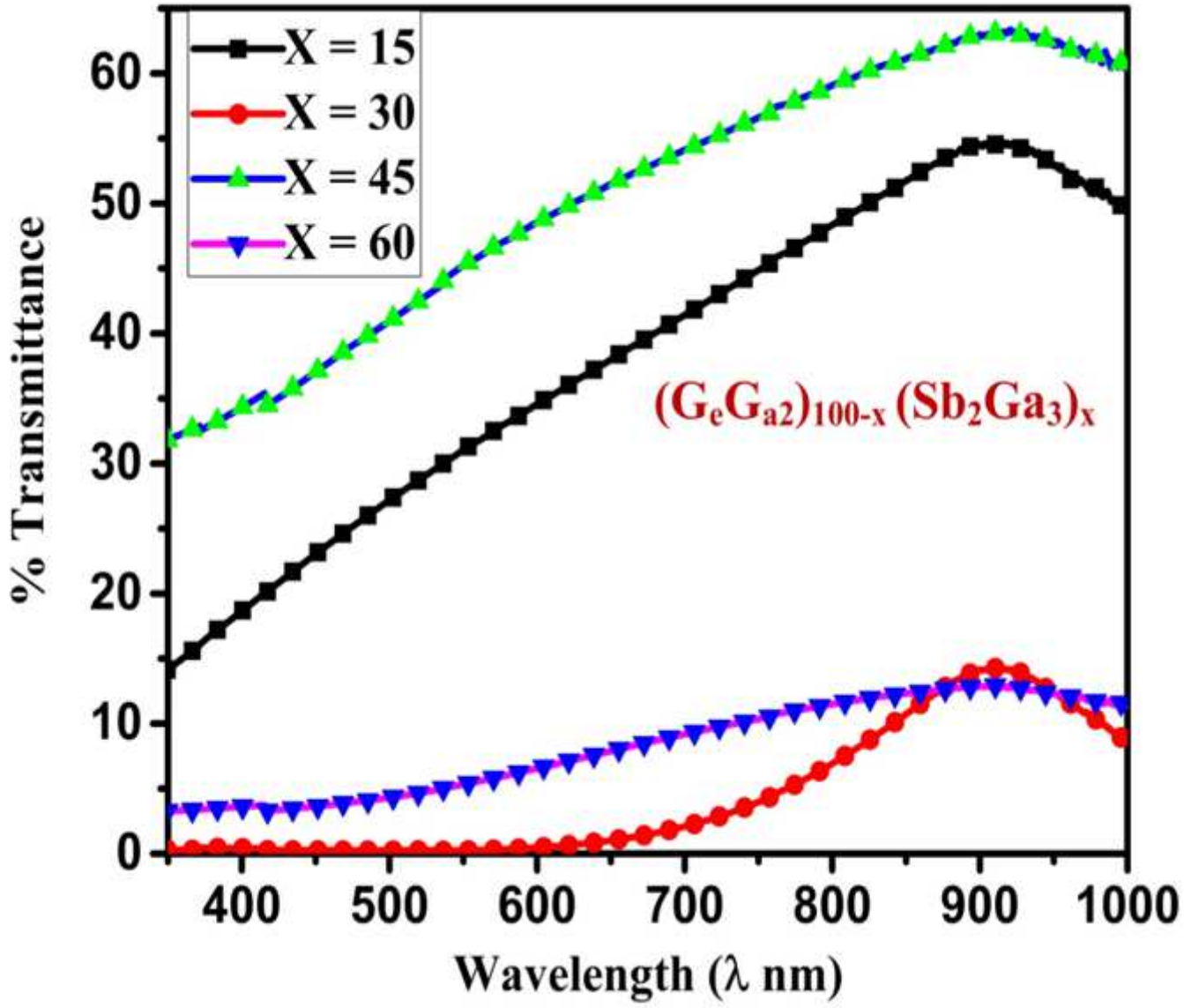

Figure 4

The spectral variation of the %Transmission for prepared thin films (GeGa2)100-x(Sb2Ga3)x for (x = 15, 30, 45, 60).

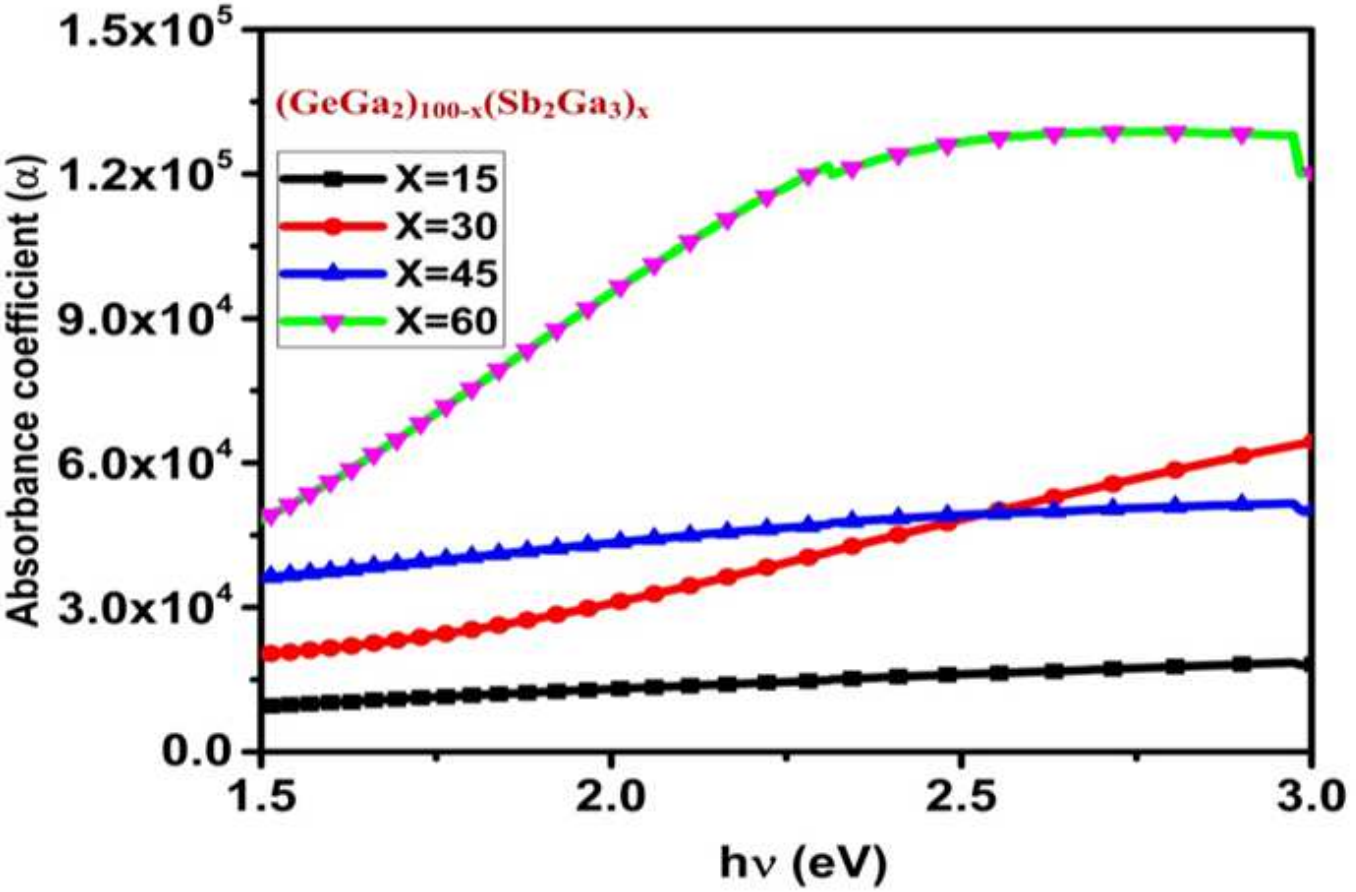

Figure 5

The distribution of “α” varies photon energy “hv” (eV) of (GeGa2)100-x(Sb2Ga3)x (x = 15,30, 45, 60).

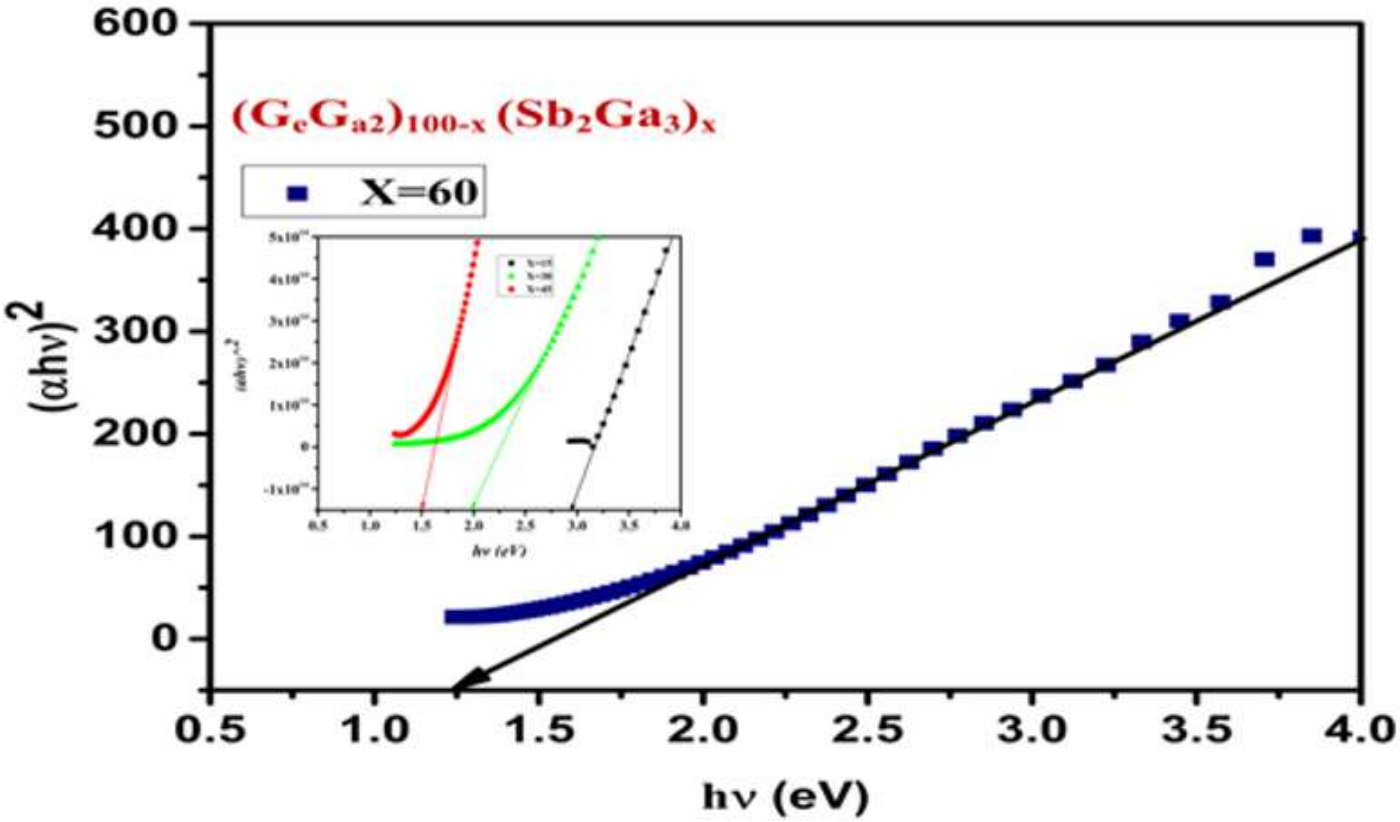

Figure 6

Variation between photon energy (hv) vs (αhv)1/n of (GeGa2)100-x(Sb2Ga3)x (x = 15, 30, 45, 60).

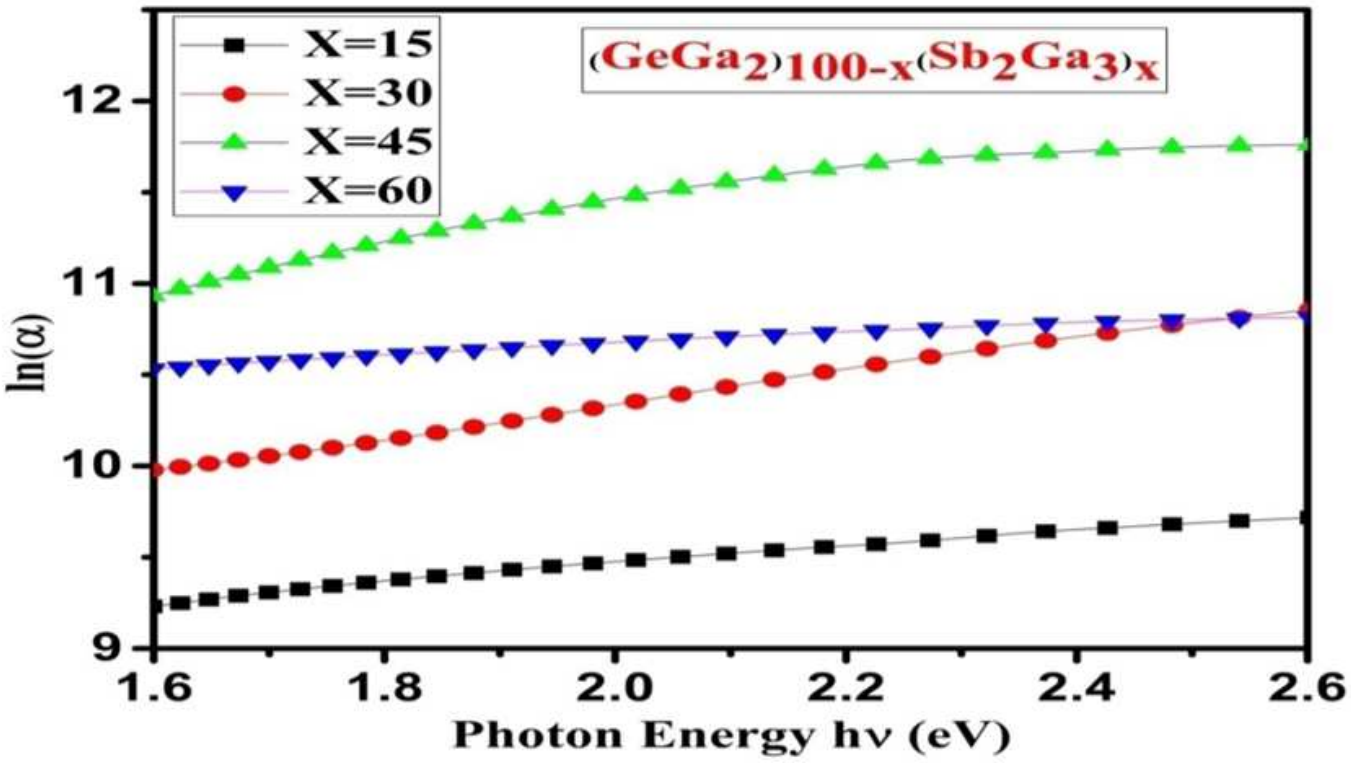

Figure 7

Varriation of photon energy vs ln(α) of (GeGa2)100-x (Sb2Ga3)x thin films glassy alloy.

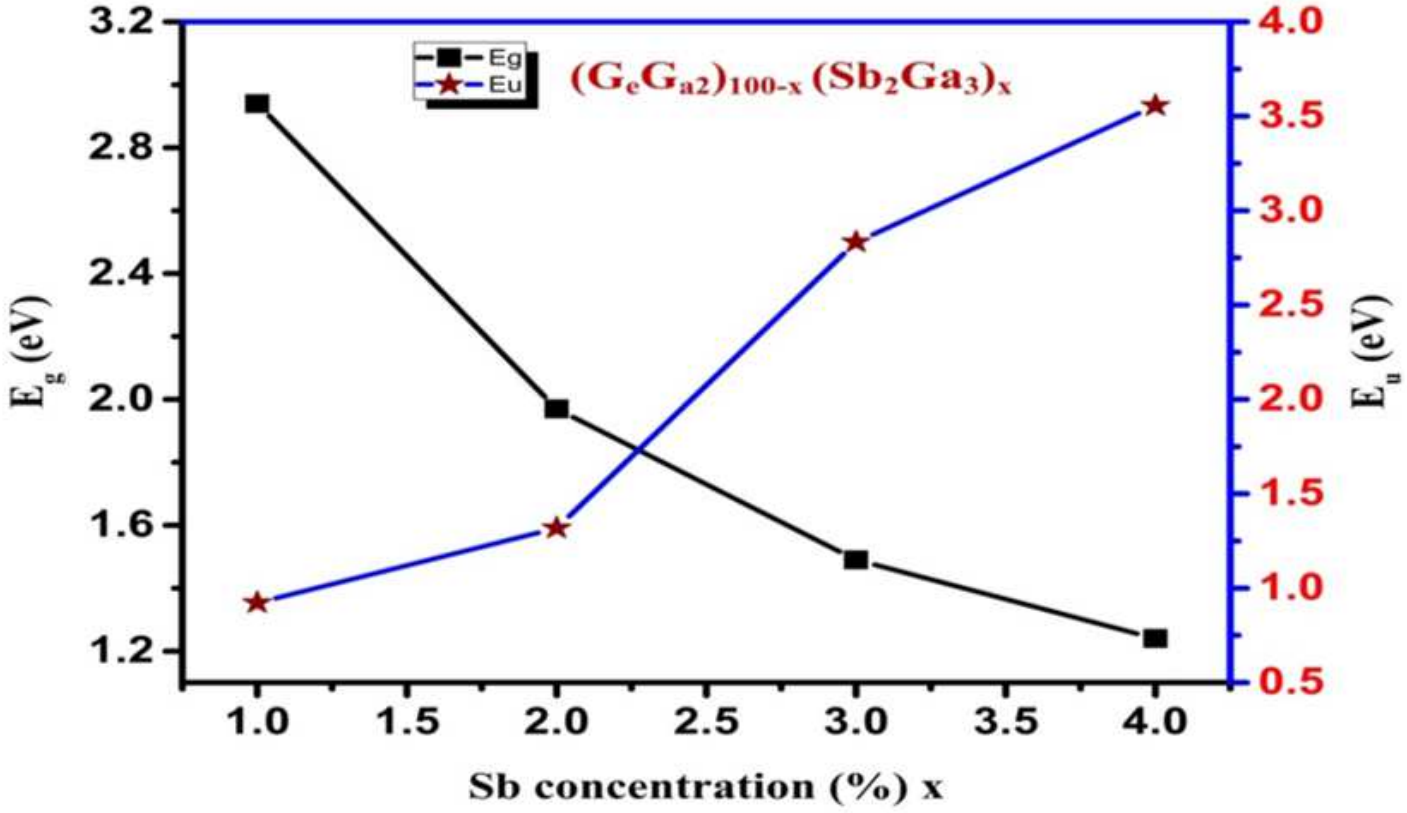

Figure 8

Shows the variation of Sb concentration Eg and Eu for (GeGa2)100-x(Sb2Ga3)x (x = 15, 30, 45, 60) Eg and Eu.

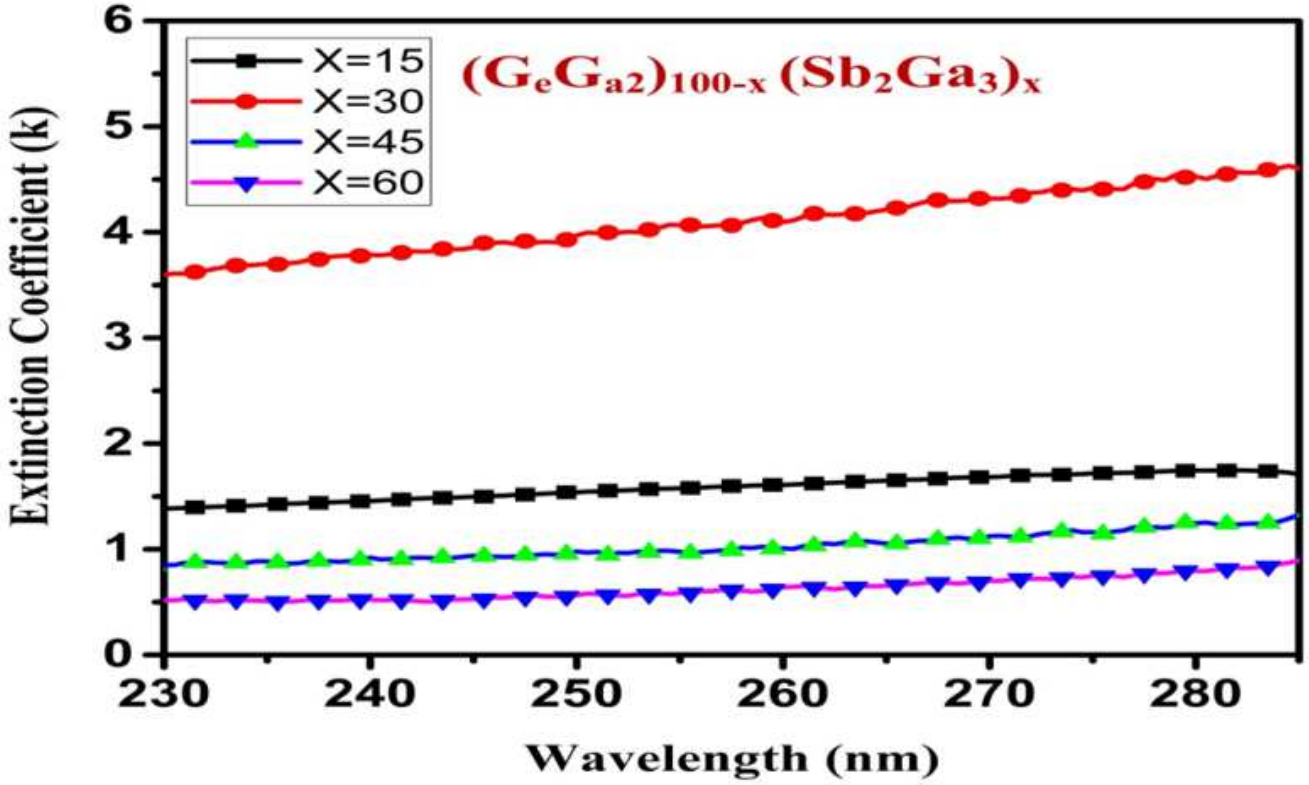

Figure 9

Variations between coefficient of extinction “k” vs wavelength “λ” of (GeGa2)100-x (Sb2Ga3)x (x = 15, 30, 45, 60).

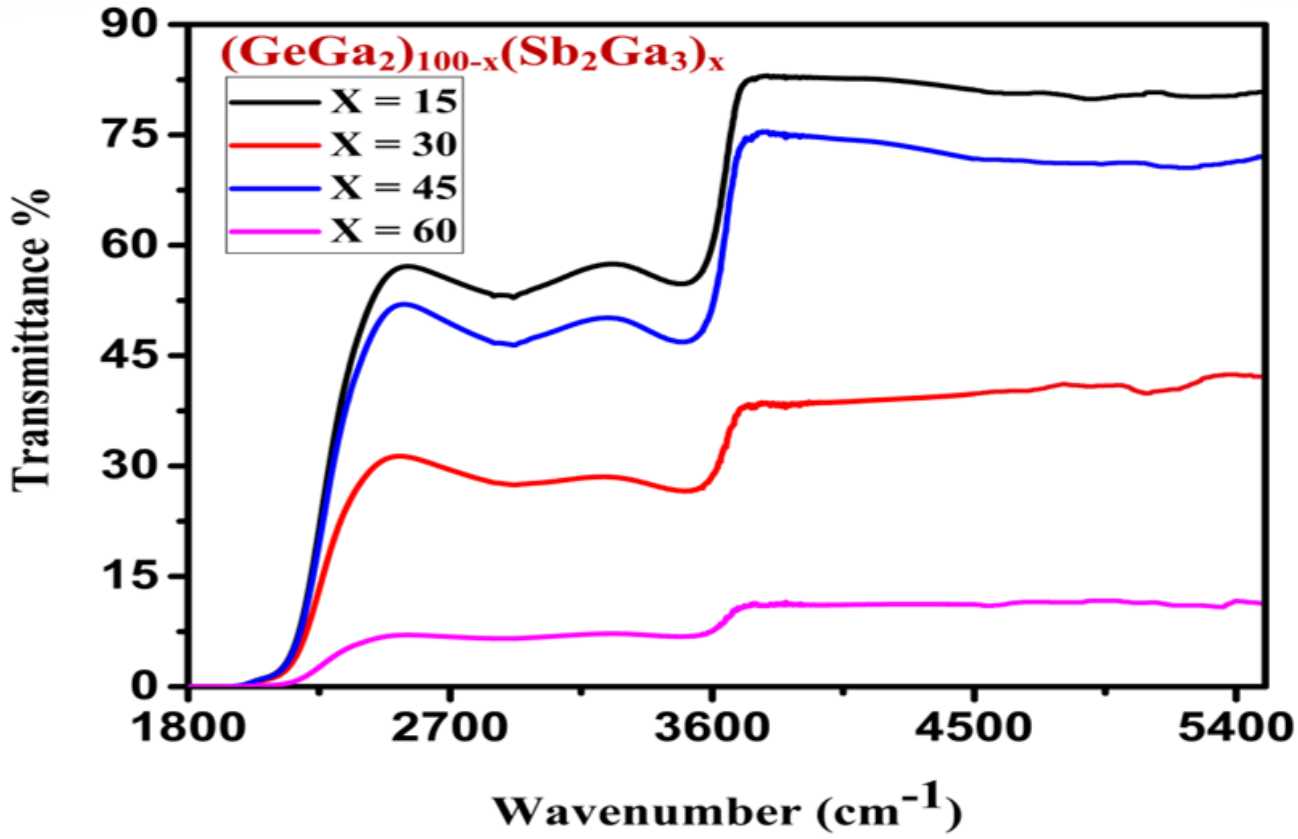

Figure 10

IR transmittance spectra of (GeGa2)100-x (Sb2Ga3)x (x = 15, 30, 45, 60) glassy thin films.